THE SLIDING HINGE JOINT MOMENT CONNECTION

Gregory A. MacRae[1], G. Charles Clifton[2], Hamish Mackinven[3], Nandor Mago[4], John Butterworth[2] and Stefano Pampanin[1]

SUMMARY

A new friction moment joint for steel framed structures is described. It has a similar cost to conventional construction and is designed such that there is negligible damage to the frame or slabs. Experimental testing shows that steel, brass or aluminium shims can provide satisfactory friction resistance and that there is almost no damage to the frame during design level displacements. A method for establishing the dependable friction force is developed considering construction tolerances and bolt moment-axial-force-shear interaction. A design methodology for the joint and a design example are provided.

1. INTRODUCTION

Seismic structural systems may be described in terms of generations [1]. Generation 0 refers to structures designed without any specific consideration for earthquake loading. Generation 1 systems are performance based designed structures to the extent that at least one performance level is specified. However methods of design and detailing to provide a specified level of performance have not been derived to match the expected demand, based on rational analysis and experimental testing. For Generation 2, designs are carried out providing sufficient detailing to meet desired performance objectives, based on rational analysis supported by experimental testing. Most modern design codes deliver Generation 2 systems, as they are based on an estimate of the demand and capacity, even if this check is carried out implicitly in the design procedure. In Generation 2 designs, the inelastic deformation generally occurs as a result of yielding within the structure as it resists the earthquake shaking. That is, the structure is damaged to protect itself, and substantial repair or replacement may be required after a major earthquake.

Generation 3 designs seek to discourage structural damage. One obvious way to achieve this goal is to design the structure and foundation to be strong enough to prevent any inelastic/nonlinear action, but this is generally uneconomic in regions of high seismicity. Other ways involve the concept of adding energy dissipating and force limiting devices to an elastically responding skeleton. This includes rocking structures in which the structure undergoes uplift, yet returns to its initial position after the shaking (e.g. Housner [2]). The use of base isolation systems containing lead and having low permanent displacements as a result of their dynamically stable bilinear hysteresis loop where the lead recrystalises over time, were developed by Robinson and Greenbank [3]. Friction devices have been available for some time (e.g. Pall *et al.* [4]) and typically have fat rectangular hysteresis loops as shown in the many frictional systems described by Christopoulos and Filiatrault [5]. Systems using supplemental viscous damping (e.g. Arima *et al.* [6]) can also dissipate energy with no permanent damage. Some modern Generation 3 systems rely on the use of unbonded post-tensioned steel to minimize permanent displacements. Precast concrete subassemblies of this type were initially tested by Cheok *et al*. [7] and they have been further developed and popularised, especially as part of the PRESSS project (e.g. Priestley and MacRae [8]; Priestley [9,10]). Some of these precast subassemblies also contain energy dissipation devices. A moment frame beam-column subassembly using post-tensioning is shown in Figure 1 where a gap opens between the beam and column face at the top and bottom of the beam depending on the loading direction.

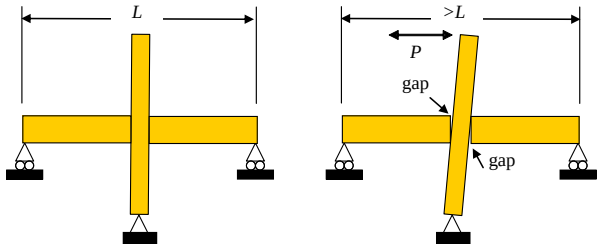

(a) Before Loading *(b) At Peak Displacement*

Figure 1: Reinforced/Prestressed Concrete Subassembly (Umarani and MacRae [11]).

Steel beam-column joint subassemblies of this type have also been considered (e.g. Danner and Clifton [12], Christopoulos *et al.* [13], Ricles *et al.* [14], Clifton [15]). They also have almost no damage to the subassembly and they can develop a so-called dissipative/recentering "flag shaped" hysteresis loops which ensure adequate energy dissipation and no permanent displacement after earthquake shaking. However, if a slab is present, either major floor damage is expected (if the slab is weak) or the desired gap-opening mechanism may be inhibited, causing extra demands on the columns (if the slab is strong). The interaction between lateral-resisting system and slab will also adversely impact on the moment rotation capacity of the joint and on the stability of the hysteresis loops under repeated cycles of loading [15]. Moreover, as the gaps open, the distance between column centrelines increases as the columns are pushed apart by the beams. This phenomenon, known in literature as "beam-growth" or "beam-elongation" [16] causes extra demands on, and possibly damage to, the columns. These slab and beam growth effects also occur to a

[1] *Department of Civil and Natural Resources Engineering, University of Canterbury, Christchurch, New Zealand*

[2] *Department of Civil and Environmental Engineering, University of Auckland, New Zealand*

[3] *Opus International Consultants, Christchurch, New Zealand*

[4] *New Zealand Heavy Engineering Research Association, Manukau City, New Zealand*

greater extent in traditionally designed Generation 2 reinforced concrete (RC) systems, where in addition to a fixed geometrical contribution to the beam elongation (due to rotation of the beam about the neutral axis), a cumulative material contribution develops due to flexural cracks not fully closing.

Generation 4 structures not only seek to have negligible damage under the design level event to the elements designed to resist the inelastic demand, they also target no damage to the rest of the frame. In Generation 4 moment frames, the beam end connections are designed as the primary element resisting inelastic demand. Moment frame connections of this type are detailed such that energy is dissipated without causing significant extension of the slab on the top of the beam, and without beam growth. A sliding hinge joint (SHJ) connection was developed over a number of years by Clifton [17, 15] to satisfy these requirements. The experimental tests of small scale components and complete joints including integral slabs have indicated stable hysteretic characteristics under constant cyclic displacements. The hysteretic shapes also indicate a self centring ability of the system. In these contributions, a detailed design procedure was developed for all the elements of the sliding hinge joint considering gravity, wind and earthquake loads [15]. Joints using similar concepts have been tested by Mander [18] and in Japan [19]. A prestressed concrete Generation 4 concrete joint using post-tensioned connections has also been developed and tested by Pampanin *et al.* [20] and Amaris *et al.* [21]. As per any innovative solution, it is desirable that Generation 4 joints can be engineered carefully to cost no more than conventional (Generation 2) construction. The steel sliding hinge joint meets this criterion, has already been used in actual construction and seems likely to be used more in the future [22].

Nevertheless, there have been questions about the durability of the steel frame with the brass shims used in tests by Clifton [15], about appropriate methods to evaluate the friction on the sliding interfaces considering construction tolerances, and about the potential to simplify the very detailed design methodology developed by Clifton for earthquake loading considerations alone. This paper was written to answer the following questions:

1) What is the sliding hinge joint and how does it behave?
2) Do shim materials other than brass exhibit desirable and stable behaviour?
3) How should the compressive force acting over the sliding surfaces be assessed?
4) How important are construction tolerances?
5) Can the detailed design methodology proposed by Clifton [15] be simplified and improved?

2. THE SLIDING HINGE JOINT

A schematic of the sliding hinge joint (SHJ) [15] is shown in Figure 2. Alternatively, the beam end may be vertically cut on an angle of about 0.10 radians so that the top flange of the beam is in contact with the column face, but the bottom flange has the "beam clearance" specified below.

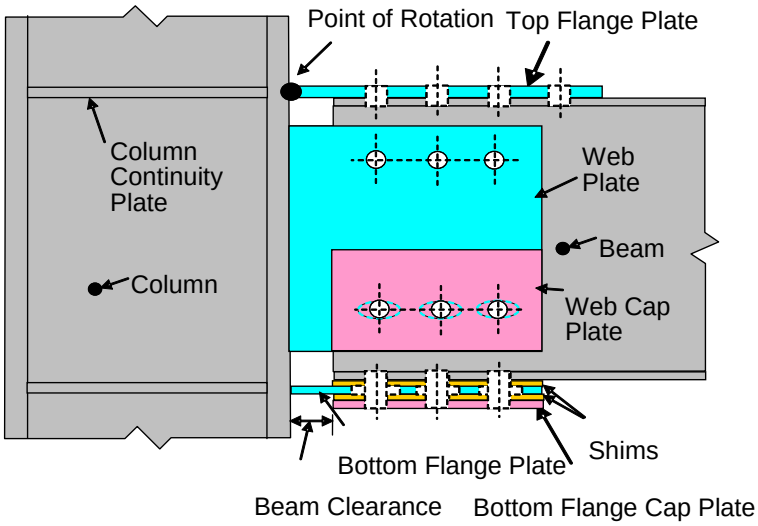

Figure 2: Sliding Hinge Joint Side Elevation (Not to Scale).

The beam end is placed a distance equal to the "beam clearance" away from the column face. This distance must be sufficient to ensure that the beam bottom flange plate flexural demands at the column face weld have no possibility of causing excessive plate or weld demands during design deformation demands. The beam top flange is connected to the column by means of a top flange plate and top flange bolts, with these sized to accommodate the overstrength sliding action from the bottom flange sliding components, thereby enforcing rotation of the beam end about the connection of the top flange plate to the column flange as shown. Because no sliding or gapping is expected between the beam, top flange plate and column, beam growth, and thus, slab damage are minimized. The shear force in the beam is carried by the top web bolts. Horizontally slotted holes are provided in the bottom flange plate and in the bottom holes of the column web plate to allow significant rotations of the beam end relative to the column face. Below the bottom flange plate is the bottom flange cap plate, which is a floating plate because it has no physical connection to the rest of the joint apart from through the bolts. A web cap plate is similarly placed on the outside of the web plate. Shims are placed on all surfaces where sliding may possibly occur. The shims have standard sized holes in them ensuring that sliding occurs on the side of the shim in contact with the bottom flange plate or the web plate. High quality control may be maintained using shop welding / site bolting techniques.

The mechanism of energy dissipation by friction is illustrated in Figure 3. Only the bottom flange friction surfaces are shown for simplicity. The column starts from rest as shown in Figure 3a. As the top of the column moves to the right, slip occurs between the bottom of the beam flange and the bottom flange plate as shown in Figure 3b. At this stage the bottom flange cap plate is not sliding because the shear force

imposed on it is relatively small. As the deformations become greater, the bolts in the bottom flange move to such an angle that they provide sufficient force for slip to also occur between the bottom flange plate and the bottom flange cap plate as shown in Figure 3c. The slip on both surfaces causes approximately twice the resistance than from one surface as shown as (c) in Figure 3f. When the loading reverses, slip initially occurs only between the bottom of the beam flange and the bottom flange plate as shown in Figure 3d, and at large displacements in the opposite direction, the bolts pull the floating plate in the opposite direction to that shown in Figure 3e, again causing an increase in lateral resistance as shown in Figure 3f.

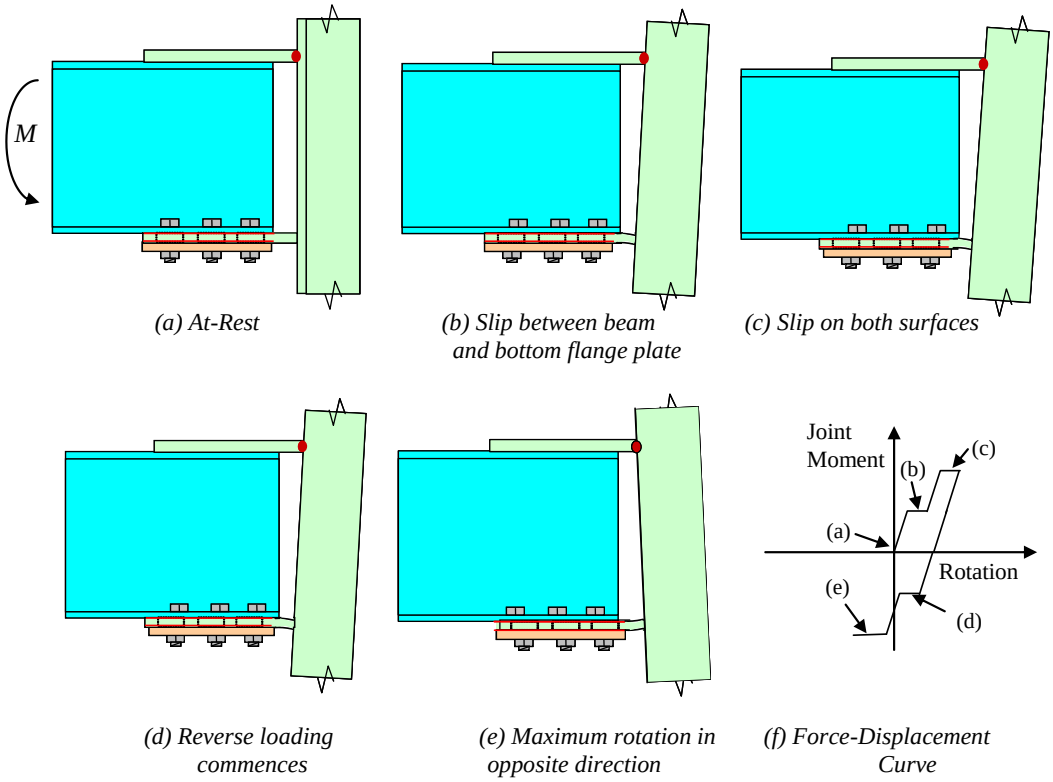

(a) At-Rest *(b) Slip between beam and bottom flange plate* *(c) Slip on both surfaces*

(d) Reverse loading commences *(e) Maximum rotation in opposite direction* *(f) Force-Displacement Curve*

Figure 3: Sliding of Plates Below Beam During Cyclic Deformations.

The frictional resistance of these connections is affected by both the shim material and the force normal to the sliding surfaces.

Pall and Marsh had found that brake lining pads placed between stainless steel pads worked well. The tests by Clifton [15] used 3mm thick brass, rather than steel, shims. This is because Takanashi *et al*. [23] and Grigorian and Popov [24] indicated that steel shims resulted in a spiky hysteresis loop with degrading strength in slotted bolted connections. Instead, brass sliding against steel provided stable hysteretic characteristics with a friction factor, μ, of 0.29 [24]. In these tests the sliding plate was between two stiff plates at a set distance apart. The authors claimed that as steel slid on steel, more particles rubbed off the surface than when steel was sliding against brass thereby increasing the difficulty of sliding. In contrast, De la Cruz *et al.* [25] found in their friction dissipater tests that steel sliding against steel shims had good behaviour and did not show large variations between the static and kinetic slip forces reported by the other authors.

The normal force over the sliding surfaces is not necessarily the load on the bolts after fully tensioning. It is also affected by the initial construction tolerances as well as by the ability of the bolts to simultaneously carry axial, bending and shear forces.

Issues relating to the shim material and the normal force over the interface are addressed in the following sections.

3. EFFECT OF SHIM MATERIAL ON BEHAVIOUR

In order to investigate the effect of shim material on the connection behaviour, joint subassembly tests were carried out using shims made of steel and aluminium, in addition to the brass shims tested initially by Clifton [15]. The test configuration is shown in Figure 4. In consideration of the negligible elongation (separation) between beam and column at the top of the beam flange, these subassemblies did not have an integral slab. The actuator applied force to the column 2.0 m above the pin at the column base, and the distance from the column centreline to the beam strut was 1.5 m. The beam centreline was 1.0 m above the pin at the column base. The end of the beam was placed 50 mm away from the column.

All steel sections and plates were from Grade 300 steel. The beam was a 360UB44.7 section with a length of 1.90m and the column was a 2.50 m long 310UC158 section. The bottom flange plate was 10 mm x 200 mm x 335 mm with 45 mm long elongated holes. The bottom flange cap plate was 10 mm x 200 mm x 240 mm. The web plate was 10 mm x 250 mm x 295 mm. The web cap plate was 16mm x 100 mm x 240 mm. The top flange plate was 12 mm x 200 mm x 340 mm. Column continuity plates were 10 mm thick. Bolts were M16 Property Class 8.8 to AS/NZS 1252 [26] and the standard bolt hole size was 18 mm. All bolts were fully tensioned in accordance with the part turn method of NZS 3404. All welds were E48XX SP. The fillet welds were applied to both sides of the plates connected to the column and had a nominal dimension the same size as the plate

thickness in order to easily develop the full yield strength of the plates. All shims were 3 mm thick. The brass shims were 70/30 cartridge brass with ½ hard tempering to AS 1566, the aluminium shims were 5005GP Series and the steel shims were cold rolled mild steel.

Figure 4: Test Configuration.

All steel sections and plates were from Grade 300 steel. The beam was a 360UB44.7 section with a length of 1.90m and the column was a 2.50 m long 310UC158 section. The bottom flange plate was 10mm x 200mm x 335mm with 45 mm long elongated holes. The bottom flange cap plate was 10 mm x 200 mm x 240 mm. The web plate was 10 mm x 250 mm x 295 mm. The web cap plate was 16 mm x 100 mm x 240 mm. The top flange plate was 12 mm x 200 mm x 340 mm. Column continuity plates were 10 mm thick. Bolts were M16 Property Class 8.8 to AS/NZS 1252 [26] and the standard bolt hole size was 18 mm. All bolts were fully tensioned in accordance with the part turn method of NZS 3404. All welds were E48XX SP. The fillet welds were applied to both sides of the plates connected to the column and had a nominal dimension the same size as the plate thickness in order to easily develop the full yield strength of the plates. All shims were 3 mm thick. The brass shims were 70/30 cartridge brass with ½ hard tempering to AS 1566, the aluminium shims were 5005GP Series and the steel shims were cold rolled mild steel.

Six tests were carried out as described in Table 1.

Table 1. Observed Effectiveness of Different Shim Materials

Test No.	Shim Material	Identifier	Interface Force to Bolt Proof Load Ratio		$V_{R,MAX}/V_{RFS}$
			At first slip, V_{Rfs}	Maximum, $V_{R,max}$	
1	Brass	4.2.2.2B	0.22	0.36	1.64
2	Brass	6.2.2.4B	0.22	0.34	1.54
3	Aluminium	4.2.2.2A	0.31	0.475	1.53
4	Aluminium	6.2.2.4A	0.25	0.385	1.54
5	Mild Steel	4.2.2.2S	0.21	0.39	1.86
6	Mild Steel	6.2.2.4S	0.22	0.365	1.66

Notes: Each test unit is identified by the notation NTFB.NTWB.NBWB.NBFB.MAT, where NTFB is the number of top flange bolts, NTWB is the number of top web bolts, NBWB is the number of bottom web bolts, NBFB is the number of bottom flange bolts and MAT is the material which may be brass (B), aluminium (A), or steel (S)

Figure 5 shows that none of the tests exhibited the traditional trapezoidal friction hysteretic curve expected by a flexible beam-column connection incorporating a traditional friction device. Also, they did not show the clear theoretical two stage increase in shear force with increasing rotation developed in Figure 3f which is evident on bolt component tests [15, 27]. Instead the hysteresis loop shapes are essentially bilinear because the double slip effect seen in Figure 3f is effectively smeared out as the bolts rotate and gradually take up the friction force.

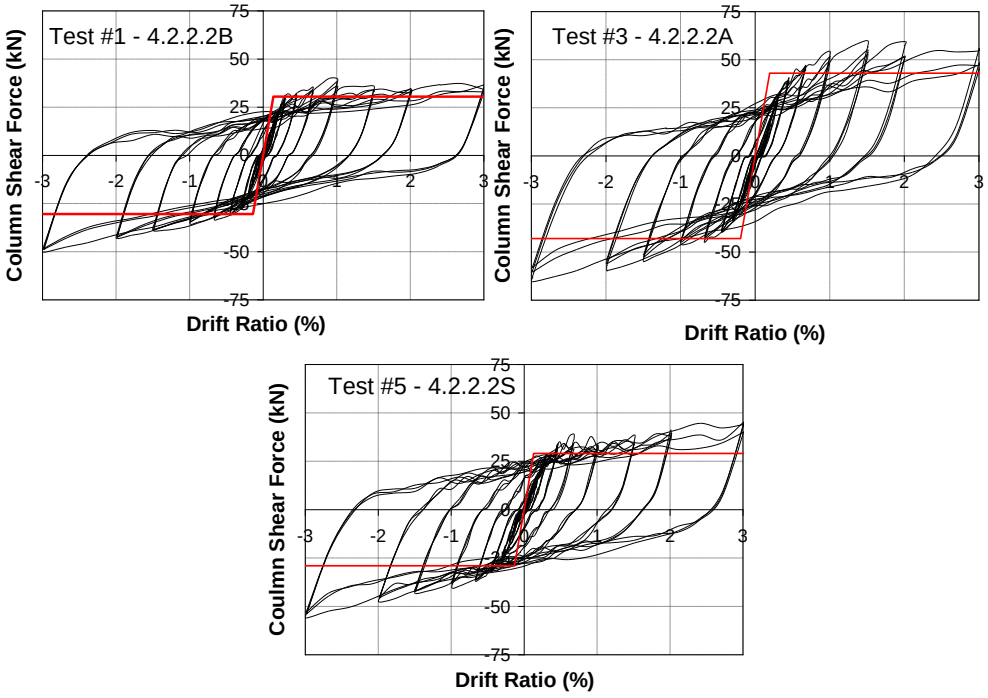

Figure 5: Column Hysteresis with Brass (B), Aluminium (A), or Steel (S) Shims and 2 Bottom Flange Bolts.

The bilinear solid lines given on the graphs have a stiffness based on an elastic beam-column centreline computer model, and the strength is that observed at first slip. This occurs at an average ratio of computed sliding surface interface force to the bolt proof load ratio in Table 1, computed based on the lower web bolts and lower flange bolt forces only. The strength at peak rotation is considerably greater than that at first slip as a result of second order deformation effects which are analogous to strain hardening. This is due to the beam prying the flange plates apart during both directions of loading. When the bottom flange is pushed toward the column, which is shown as negative displacement in the

graphs, then the bottom flange plate is in compression increasing the friction forces as a result of Poisson's swelling of the plate. More importantly though, the bottom flange plate cap yields in flexure during these negative displacements as the bottom flange plate becomes concave downwards as seen in experimental tests. During positive rotation the cap plate is not subject to this bending. Clifton [15] shows that this effect is not as significant in subassemblies with floor slabs, because, during positive rotation, the concrete bears against the face of the column, raising the point of beam rotation above the top flange thereby increasing the moment capacity to a similar extent of strength seen in the negative loading in these tests, such that the increase under both positive and negative moment is similar.

Tests with steel and brass shims indicated relatively stable behaviour whereas the aluminium test indicated a decrease in strength after the first cycle to each displacement. Peak strengths were up to 86% greater than these values as seen in Figure 5 giving the values in Table 1. These usually occurred for a very short time at the peak displacement in the negative displacement direction.

The steel and brass shim tests indicate similar force ratios. The fact that there was very little stiffness degradation with the steel and brass shim tests indicates that the beam clearance (i.e. the distance from the beam end to the column face) was sufficient to prevent significant joint performance deterioration such as has been seen in tests with shorter clearances [15]. Also, undesirable peaks and reductions in the force-displacement response of the sliding subassemblies reported by Takanashi *et al.* [23] and Grigorian and Popov [24] were not seen in this study. This is due to the asymmetric sliding condition of these joints as shown in Figure 3 compared with the sliding condition of the Grigorian and Popov [23] tests in which the sliding forces and the sliding deformations on either of a central plate are the same. It is interesting to note that Grigorian and Popov, in discussion with a tribologist, had indicated that the friction coefficient of brass against steel was 0.29, while that of steel against steel is generally greater, in the region of 0.30 to 0.35. Since the friction force across an interface is a function both of the friction coefficient and the normal force over the interface, it is conjectured that with the asymmetric sliding connection in its stable sliding condition, the normal force over the interface is less for steel than it is for brass as a result of the MVP interaction. This leads to a similar sliding shear capacity per bolt, as shown in Figure 5, and each shim material generates hysteresis loops of similar stability over successive cycles, in contrast to the use of the softer aluminium shims.

The use of steel shims has three major advantages. Firstly, steel is cheaper and more readily available than brass. Secondly, since steel shims are not a dissimilar metal to the other steel components, the propensity for corrosion would be expected to be less severe. Thirdly, the steel shims can be tack welded into position onto the steel beams and cap plates for ease of erection. For these reasons, steel shims have been used in recent SHJ building construction [22].

The force ratio obtained with the aluminium shims is greater than for the brass or steel shims. However, the strength for the tests with aluminium shims decreased after the first cycle in the test, and the interface force to the bolt proof load ratio was significantly lower in the second test than in the first test. This is because the material on the surface of the shim moved during the testing as shown in Figure 6. Figure 6a indicates the beginning of the test. When the bolt, and the beam flange, move in one direction then the aluminium material increases in height around the bolt. Moving in the other direction, the material is also higher on the other side of the bolt causing a raised up area near the bolt hole as shown in Figure 6d.

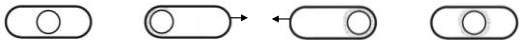

(a) *(b)* *(c)* *(d)*

Figure 6: Formation of Elevated Aluminium Impressions from Slotted Holes.

The joint was essentially undamaged after each test, so the shims could be removed and the next test could be conducted. Furthermore, the permanent displacements are likely to be small because of the high post-elastic stiffness (MacRae [28], Kawashima *et al.* [29]) implying that the structure is unlikely to require straightening after the earthquake. Preliminary time history analysis by Clifton [15] indicated that permanent displacements were small enough to fall within the constructional tolerance envelope of the New Zealand Steel Structures Standard, NZS 3404 [30]. Additional springs to further increase the restoring force characteristics, as described by Clifton [15], enhance the post-earthquake self centering and joint elastic stiffness however the cost-benefit of such systems requires careful assessment.

4. CONSTRUCTION TOLERANCES

Because there are rolling tolerances on beams and plates, the top and bottom flange plates connected to the column flange must be offset vertically to allow for these. However it is also essential that these plates not be placed too far apart. If they are, then even when the bolts are tightened, these plates may not come into full contact with the beams thereby reducing the shear friction force that can be transmitted across the interface. In the worst instance of no contact, in theory only one half of the available friction force would be obtained because friction would only occur on the side of the column plates touching the floating (cap) plates. For the full bolt force to be transferred in compression across the interfaces, then the top and bottom flange plates, shims and beam should have a tight fit. Any gap will require force from the bolts to close, and this force will reduce the initial normal compression over, and the sliding resistance of, the interface. The clear length of bottom flange plate from the column face should be at least "the weld size + (0.0375 x the beam depth) + 2.5 times the bottom flange plate thickness" [15]. This method was developed in order that when the sliding hinge joint is subject to maximum design negative rotation as shown in Figure 3(c), the clear length of bottom flange plate between its attachment to the column and its clamping by the beam is sufficient to prevent excessive loss of both bolt tension and sliding shear capacity. This empirical method has been shown to be satisfactory in large scale tests by Clifton [15] as well as those undertaken by Mackinven [31]. For the models tested, this is 10 mm + 0.0375 * 360 mm + 2.5 * 10 mm = 48.5 mm, which is close to the 50 mm beam clearance provided. Clifton proposes construction tolerances such that the total unfilled gap between the beam top and bottom flange plates should not exceed 2 mm.

In the discussion below, expressions are developed to evaluate the change in connection initial frictional moment resistance as a function of the gap size, for small member deformations. At large displacements, the increase in strength due to the second-order deformations, as described above, are not considered. It is assumed that the top and bottom flange bolts are initially tightened, and the web plate bolts are tightened later.

If the top and bottom flange plates are flexible, parallel to the elements they are connecting, placed further apart than need be, and bend in double curvature, then the deformed shape

will be as given in Figure 7. On the bottom flange plate bending occurs between the weld and the end of the cap plate which is at the end of the beam, L_{bot}. On the top flange plate bending occurs between the weld and the side of the bolt head of the first row of bolts, L_{top}. The top and bottom beam flanges will also bend as shown in Figure 8 over the distance, $L_{d,}$ between the end of the root radius and the side of the bolt head. The modes of deformation described above all contribute to the loss of compression over the beam-bottom flange plate sliding surface.

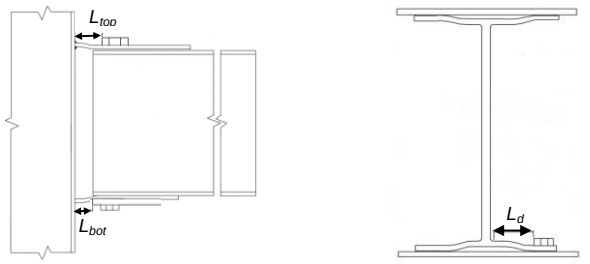

(a) Elevation *(b) Cross-Section*

Figure 7: Flange Plates Bending in Double Curvature.

The force due to the tolerances, P_{tol}, over the connection to close the gap, Δ, may be considered as acting in series between the top flange plate, the beam top flanges (which are in parallel), through the beam web, through the beam bottom flanges (which are in parallel), and through the bottom flange plate. The plates are conservatively assumed to bend in double curvature and to have shear flexibility. The two modes (bending and shear) can be considered to act in series. For any member in double curvature over a clear length, L, the flexural stiffness is K_b (= $12EI/L^3$) and the shear stiffness, K_s (= GA_s/L). The relationship between P_{tol} and Δ is given in Equation 1, where the section shear area A_s is taken as being equal to 5/6A, where A is the plate area. The second moment of area, I, of the member is found using the standard effective width, b_{eb}, in Equation 2, where the symbols are defined in Figure 8. Yielding of the plates will provide an upper bound to the forces from these equations as will be shown later.

$$\Delta = \frac{P_{tol}}{K_b} + \frac{P_{tol}}{K_s} \tag{1}$$

$$b_{eb} = \min\begin{cases} S \\ 2\left(a - k + \dfrac{t_{wb}}{2}\right) \end{cases} \tag{2}$$

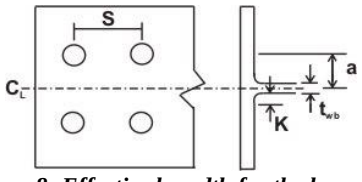

Figure 8: Effective breadth for the beam flange.

The force, $P_{tol,}$ to close a gap, Δ, considering the whole load path described above, is therefore given in Equation 3, where the notation *tfp* stands for top flange plate, *btf* is beam top flange, *bbf* is one side of the beam bottom flange, and *bfp* is one side of the bottom flange plate. It should be noted that the different sides of the top and bottom beam flanges are in parallel and this is indicated by the presence of the "2", below.

$$P_{tol} = K^*\Delta \tag{3}$$

$$K^* = \frac{1}{K_{tfpb}} + \frac{1}{K_{tfps}} + \frac{2}{K_{btfb}} + \frac{2}{K_{btfs}} + \frac{2}{K_{bbfb}} + \frac{2}{K_{bbfs}} + \frac{1}{K_{bfpb}} + \frac{1}{K_{bfps}}$$

The interface between the bottom flange plate and the bottom cap plate will have the fully tensioned load from the bolts applied over it in compression, P_{proof} (= $2n_bN_{tf}$), while the compression over the interface between the bottom flange and the bottom flange plate, P_{intbf}, is the fully tensioned load from the bolts, P_{proof}, reduced by P_{tol}. Here n_b is the number of bolts in the bottom flange and N_{tf} is the minimum bolt tension at installation, which was taken as the proof load of one bolt. The loss of sliding resistance, as a ratio of the sliding resistance with no gap to that with a gap, α, considering the summation over both interfaces is given in Equation 4. That is, if α = 0.1, then 10% of the connection frictional strength is lost as a result of friction. Values greater than 50% are not appropriate as it means that the force to close the gap is greater than the fully tensioned load from the bolts. Also, values of P_{tol} which cause the plates to yield may put a lower limit on the maximum reduction in force as shown in the example below.

$$\alpha = 1 - \frac{\Sigma P_{\text{int}bf}}{\Sigma P_{proof}}$$

$$= 1 - \frac{P_{proof} + \left(P_{proof} - P_{tol}\right)}{2P_{proof}} = \frac{P_{tol}}{2n_bN_{tf}} \tag{4}$$

For example, for the 2/3 scale SHJ subassembly Test No. 6 from Table 1 with the 360UB44.7 beam shown in Figure 4 the spacing between holes in both directions, *s* and *a*, were both 70 mm, and there was 50 mm between the centreline of the last holes and the end of the beam. The maximum diameter of the bolt head or nut is 2/√3 x 27 mm = 31 mm, where 27mm is the across-flats distance. Six M16 Grade 8.8 bolts (3 each side of the web) were connected to the top flange plate, and four bolts (2 each side of the web) were connected the bottom flange to the bottom flange plate.

Deformation of bottom flange plate. The beam clearance (see Figure 1), c_b, was 50 mm and 12 mm fillet welds were used between the column flange and bottom flange plate. The clear length of bending bottom flange plate, $L_{bot,}$ was therefore 38 mm. The bottom flange plate thickness, t_{bfp}, was 10mm and the breadth, b_{bfp}, was 200 mm. Therefore K_{bfpb} was 729x10^6 N/m and K_{bfps} was 3,509x10^6 N/m.

Deformation of top flange plate. The distance from the column face to the centreline of the first row of top flange bolts, c_t, was 100 mm. The clear distance of the top flange plate, $L_{top,}$ was therefore 100 mm – 12 mm – 31 mm/2 = 72.5 mm, where 12 mm is the fillet weld size. The top flange plate thickness, t_{tfp}, was 12mm and a breadth, b_{tfp}, was 200 mm. Therefore K_{tfpb} was 181x10^6 N/m and K_{tfps} was 2,206x10^6 N/m.

Deformation of flanges. The beam flange thickness, t_f, is 9.7 mm, while the web thickness is 6.9mm and the root radius is 11.4 mm. Therefore the clear distance either side of the flange, L_d, is 70 mm/2 – 6.9 mm/2 – 11.4 mm – 31 mm/2 = 4.65 mm. An effective width of the clear span plus the maximum bolt head diameter of 31 mm + 2 x 4.65 mm = 40.3 mm is used for each of the bolts in each flange. Since there were 3 bolts on each side of the top flange and 2 bolts on each side of the bottom flange, K_{btfb} was 219,000x10^6 N/m, K_{btfs} was 16,813x10^6 N/m, K_{bbfb} was 146,000x10^6 N/m and K_{bbfs} was 11,200x10^6 N/m. These stiffnesses are much more than that of the flange plates, so they will not have a significant influence.

For a tolerance of Δ = 2 mm x 2/3 = 1.33 mm for the 2/3 scale unit, the force required for closing the gap, P_{tol}, and the loss of strength computed using Equations 3 and 4, α, is:

P_{tol} = $K^*\Delta$ = 0.001333 m * 126 MN/m = 168 kN

$$\alpha \quad = \frac{P_{tol}}{2n_b N_{tf}} \quad = \frac{168kN}{2*4*95kN} \quad = 22\%$$

Of this displacement, 75% is from the deformation of the top flange plate, and 21% comes from the deformation of the bottom flange plate, with the remaining 4% from the deformation of the beam flanges. Here P_{tol}/P_{proof} = 168kN/(4*95) = 44% implying that the force required to close the crack is a substantial proportion of the fully tensioned load from the bolts across the sliding surfaces. For other test units, like Test #5, with only 2 bolts in the bottom flange, α is approximately twice the value computed above indicating that about 44% of the joint capacity is likely to be lost.

The above assumes elastic behaviour of the flange plates. The maximum reduction in strength in the plastic case is limited by the plastic flexural capacity of the column flange plates. For the top plate the maximum shear force that the plate can carry is $V_{t,max}$ computed as the moment capacity, M, divided by the distance to the point of contraflexure which is $L_{tclear}/2$. Since the section plastic moment capacity, M_{px}, of $F_y(bd^2/4)$ = 300 MPa x ((12 mm)^{2}x200 mm/4) = 2,160 kNmm, $V_{t,max}$ = 2,160 kNmm/(72.5mm/2) = 60 kN. For the bottom 10 mm thick plate with a clear span of 38 mm, $V_{b,max}$ = 79 kN. Both of these forces are much less than the expected force if the plates remain elastic, P_{tol}, of 168 kN. The top flange controls, so that the maximum decrease in force over the connection is 60 kN. (Note that if the top connection is buried compositely into a slab, then the bottom flange will control the strength). In many connections this plastic limit is likely to control the strength. If single, rather than double, curvature bending is assumed, then a lower, and less conservative, reduction in strength will be obtained. The decrease in strength, P_{tol}, is 60kN. This is associated with a strength decrease, α, of

$$\alpha \quad = \frac{P_{tol}}{2n_b N_{tf}} = \frac{60kN}{2*4*95kN} = 10.5\%$$

In the computation above, double curvature of the bottom plate was assumed. If there is significant rotational flexibility at the bottom flange plate to column connection, then the assumption of single curvature behaviour may be more appropriate. This would halve the value of α obtained above. Furthermore, the effect of moment-axial force interaction on the column flange plate has been ignored in the computation above. For a rectangular plate, simple plasticity theory shows that the effect of axial force is given as $M_{px}(P) = M_{px}(1 - (P/P_y)^2)$. For the cases we studied, the decrease in moment capacity due to axial force was less than 15% even when there are 6 bolts in the bottom flange. Considering these factors, the strength decrease α may be as low as 4.5%. Finite element studies described by Clifton, with continuity plates included, indicate that the loss in strength is about 6%. This effect is small enough to be ignored for beams detailed to maintain the maximum tolerance gap at around 3mm.

The loss of strength computed above is based on the assumption that sliding has not yet started. As rotation of the joint occurs, the column flange plates need to deform. As they yield, a stable sliding mechanism occurs, and effects of the initial tolerances disappear. This has also been confirmed by finite element analysis [15].

5. EFFECT OF BOLT M-V-P INTERACTION

The bolt deformation and bearing areas on the bolt shank are idealised in Figure 9. Horizontal forces on the plates and beam touching the bolt, as well as the forces on the bolt itself are given in Figure 10. It may be seen in Figure 10b that in addition to the bolt prestress force (shown by the dotted blue arrows), another force, R, is required for equilibrium. While this seems to indicate an increase in bolt axial tension force, such a force cannot be realised if the bolt is already at yield in tension. The normal force that can be imposed by the bolt on the plates is reduced by the bending and shear forces which the bolt must also carry as it is forced into double curvature. The reduction in bolt tension from the as-installed condition for stable steel on brass is around 40% [15].

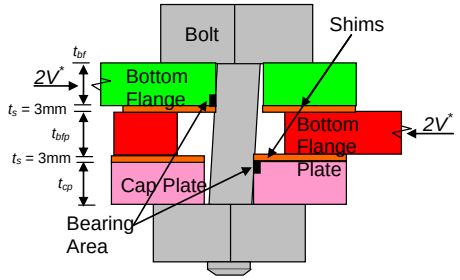

Figure 9: Idealized Bolt Deformation, External Horizontal Forces and Bearing Areas on Bolt Shank.

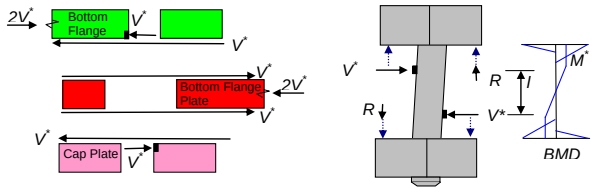

(a) Horizontal Forces on Plates *(b) Bolt*

Figure 10: External Forces on Components.

Equation 5 is used to account for the moment-shear-axial force interaction for each bolt which affects the interface force. The magnitude of shear force carried by each bolt is simply V^*, the friction force over each surface. The moment demand in the bolt at the critical location shown in Figure 10b is M^* which is $V^*l/2$, where l is the distance between the centroids of the force imposed by the bottom flange and cap plate shown in Figure 10b. It is taken as t_{bfp} + 3 mm/shim x 2 shims + 0.2d, where d is the bolt diameter. M_{rfn} is the bolt moment capacity considering axial force interaction, V_{rfn} is the bolt shear capacity considering no axial force interaction. S_{fn} is the plastic section modulus of the circular section of the core area. Both V_{rfn} and M_{rfn} may be approximated from the nominal bolt diameter, d [15]. The 0.2d represents the sum of the depths of the bearing zones on the plates at each end of the bolt shown in Figure 9. It was initially assumed, then found to match the depth of bearing zone given by Clifton and matches the physical depth of bearing zone from his small scale component tests. The friction coefficient μ was confirmed as 0.29 for both the brass shims by Clifton. For the steel shims the friction coefficient μ was taken as 0.30. (As previously noted the behaviour of both shims was similar). For high strength bolts the nominal ultimate tensile stress, f_{uf} is 830 MPa and the fully tensioned bolt load, N_{tf}, is given in design tables as the proof load. Equation 5 may be solved to obtain the axial force N^*, and shear force V^*, that can be resisted in the bolt. The connection force is $2V^*$ as shown in Figure 10a.

$$\left(\frac{M^*}{M_{rfn}}\right)^{1.71} + \left(\frac{V^*}{V_{fn}}\right)^{1.71} < 1 \qquad (5)$$

$$V^* \quad = N\mu \qquad (6)$$

$$M^* = \frac{V^* l}{2} = \frac{N\mu l}{2} \qquad (7)$$

$$M_{rfn} = S_{fn}\left(1-\frac{N}{N_{tf}}\right)f_{uf}$$

$$\approx 0.1665d^3\left(1-\frac{N}{0.56d^2 f_{uf}}\right)f_{uf} \quad (8)$$

$$V_{fn} \approx 0.62 f_{uf} \times 0.56d^2 \quad (9)$$

Component tests were conducted for comparison with the equations above using M24 bolts, M30 bolts and different combinations of bottom flange plate thickness, cap plate thickness and beam flange thickness [15]. The component test configuration is shown in Figure 11. Here, the right hand side with the reaction beam and SHJ cleat (which is equivalent to the bottom flange plate) is moved horizontally relative to the left hand side with the beam flange stub. Friction occurs over the two surfaces with 3mm brass shims.

The computed sliding force per bolt per interface normalized by the fully tensioned load from the bolts found using Equation 5 is shown in Figure 12. Tolerance issues were not considered in these calculations, so the computed normalized sliding force divided by the fully tensioned load from the bolts if there were no moment-shear-axial force interaction is simply the friction factor of 0.29 for brass shims or 0.30 for steel shims. The calculated behaviour indicates a decreased sliding strength with increasing bolt lever arm because the moment demands are greater due to the greater normalized lever arm, *l*, shown in Figure 10. This is because the greater moment demands cause greater moment-shear-axial force interaction, reducing the normal force applied by the bolt, and therefore the friction force over the sliding interfaces. Testing at rates of up to one cycle per second at ± 0.030 radians of rotation indicated negligible difference in behaviour.

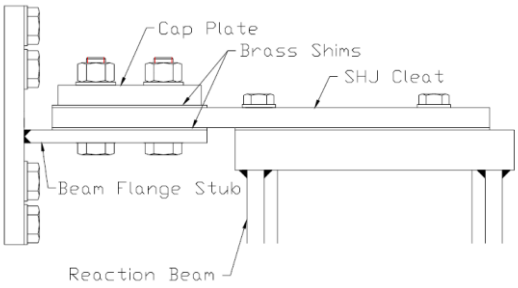

(a) Idealization

(b) Actual situation showing reaction beam, flange plate and test setup

Figure 11: Component Test Configuration [15].

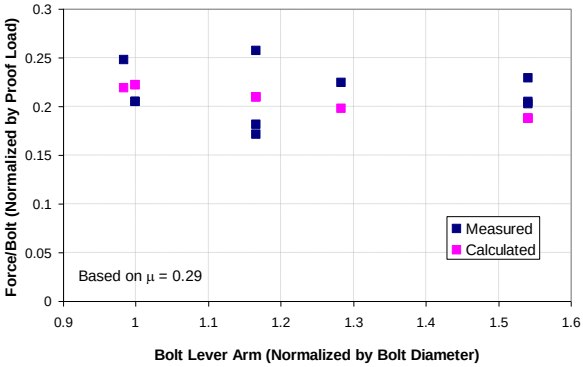

Figure 12: Measured and Computed Component Test Strengths (Brass Shims).

The measured sliding strength is shown on the same graph. Here, the strength at zero displacement during the cycles at the fifth loading step (i.e. to the design level displacement) was taken as the sliding strength because some of the earlier cycles had slightly higher strengths due to overcoming initial friction. The strength has a tendency to decrease with greater bolt lever arm, but the tendency is not as much as that computed. The sliding strength as measured is about 1.2 times that calculated and this should be considered in capacity design considerations. Other results of subassemblies incorporating Belleville springs as well as finite element studies [15] indicate that the behaviour matches the calculated strength well.

For the tests described in Table 1 the bolt lever arm divided by the bolt diameter was 1.18 [32]. Substituting Equations 6 to 9 into Equation 5 results in the quadratic solution for N given by Equation 10, where a = -2.880μ, b = 1.68168 $\mu f_{uf} ld$ + 1.613μ $f_{uf} d^2$ + $f_{uf} d^2$, and c = -0.56 $f_{uf}^2 d^4$.

$$aN^2 + bN + c = 0 \quad (10)$$

After the quadratic has been solved for N, the normalized sliding force, μ_n, may be computed from Equation 11 as 0.20 for brass or steel shims. This is consistent with the measured normalized forces of 0.21 to 0.22 (for brass and steel shims) given in Table 1, and with the computed and experimental sliding forces from the subassembly tests in Figure 12. If less care had been taken with tolerances during construction, possibly lower forces would be obtained. Equation 5 provides a good estimate of the normal force over the interface for computing the sliding shear forces which should be appropriate for design.

$$\mu_n = \mu N / N_{proof} \quad (11)$$

6. DESIGN METHODOLOGY

1. The point of rotation for design of the joint is taken at the top of the steel beam. This is obvious for the case where the concrete slab is separated from the column flanges. When the slab is in contact with the column flanges and is in compression, then the initial sliding strength is slightly increased, but the strength at large rotations is similar to that for loading in the reversed direction where bending of the bottom flange cap plate also contributes to the strength.
2. Select initial beam and column sizes based on preliminary considerations of strength and stiffness.
3. Column flange and web plates, as well as floating plates, should have a similar, or slightly greater thickness than the flange or web to which they are connected and the

flange plates should also be wider than the beam flange to ensure that they are flexible but don't yield in axial tension under the overstrength demands.

4. Elongated holes in the bottom flange plate should accommodate a rotation of 0.0375 radians in each direction.

5. The gap between the beam end and the column face is determined as weld size + (0.0375 times the beam depth) + 2.5 times the bottom flange plate thickness.

6. The connection of the column plates to the column should be sufficient to ensure that if inelastic deformation occurs, it will all occur in the plate rather than in the weld.

7. The overstrength factor for the beam is computed. The average increase in strength of the beam-column joint tests with steel shims above the observed sliding strength in Table 1 was 1.76. The observed design strength (related to a normalized bolt shear of 0.22 as shown in Table 1) was therefore 1.10 times the computed strength (related to a normalized bolt shear of 0.20 as a result of MPV interaction). The peak strength is therefore 1.76 x 1.1 = 1.93 times the computed sliding strength. An overstrength factor considers not only the increase in strength of the inelastic element, but also the likely strength of the elements to be protected from yielding. Tests indicate that typical steel elements typically have an actual minimum yield strength of more than 1.14 times the nominal value, and more than 1.14/0.90 = 1.27 times the dependable strength, where 0.9 is the strength reduction (or resistance) factor for design of steel members [15]. The overstrength, ϕ_{oms}, is therefore computed as 1.93/1.27 = 1.5. This reflects the fact that the capacity of the elements designed to resist overstrength actions may be based on their ideal (or nominal) capacity rather than their design capacity in order to provide a strength hierarchy rather than provide absolute protection against inelastic demand in the elements designed to resist the overstrength actions. The maximum computed sliding flexural strength, $M_{slide,max}$ should therefore be less than approximately M_n/ϕ_{oms} where M_n is the section (nominal) flexural capacity.

8. Compute the (normalized) design sliding shear capacity for each bolt considering moment-shear-axial (MVP) interaction with Equations 10 and 11.

9. The nominal (or ideal) moment capacity of the joint, M_{slide} is computed according to Equation 12 where N_R is the number of rows of bolts used to resist bending in the lower web, N_{Bi} is number of web bolts in each of these rows, N_{BF} is the number of bolts in the bottom flange, h_i is the distance from the rotation point to each row of bolts, h_f is the distance from the rotation point to centre of the bottom flange plate, V_{ij} and V_k are the shear strengths caused by friction on the two sliding surfaces. These consider MVP interaction.

$$M_{slide} = \sum_{i=1}^{N_R}\sum_{j=1}^{N_{Bi}} V_{ij} h_i + \sum_{k=1}^{N_{BF}} V_k h_f \qquad (12)$$

10. The dependable design, $M_{des,}$ is $\phi M_{slide} = 0.9 M_{slide.}$

11. Sufficient top flange bolts are provided to carry the horizontal force from the bottom flange bolts and web bottom bolts.

12. The beam seismic shear force demand may be determined as $\phi_{\text{oms}} M_{slide}$ divided by the distance to the beam point of inflection. The top web bolts and web flange plate should be checked using standard methods to ensure sufficient capacity. Tolerances are controlled by ensuring that the beam is bolted to the column plates when the welding of these plates to the column flange is carried out in the factory. The sequence of the construction is that flange bolts should be tightened before the web bolts are tightened. This minimizes the deformation and loss of strength in the sliding plates. The moment applied to the column and panel zone design should be computed using the connection overstrength moment value. Also, the panel zone is strengthened, if needed, to ensure that it will not be the weakest link in the frame.

7. DESIGN EXAMPLE

1. The point of rotation is the top of the beam.

2. Beam and column sizes initially selected are Grade 300 360UB44.7 and 310UC158 sections as used in the test described previously. Bolts are M16 Property Class 8.8 to AS/NZS 1252.

3. The column flange and web plates are made 10mm thick, as the beam flange was 9.7 mm thick.

4. Elongated holes in the bottom flange plate have a length of 360 mm x 2 x 0.0375 rad + 18 mm = 45 mm, where 360 mm is the distance from the point of rotation to the bottom flanges and 18 mm is the nominal hole diameter for the 16 mm diameter fastener.

5. The minimum gap between the beam end and the column face is 10 mm + 0.0375 * 360 mm + 2.5 * 10 mm = 48.5 mm. For design 50 mm is used.

6. A 10 mm fillet weld all around the column plate to column flange connections is required to ensure that the weld will not yield.

7. The nominal section moment capacity, $M_n = Z_{ex}F_y$ = 770,000 mm^3 x 320 MPa = 246 kNm. Therefore $M_{slide,max} = M_s/1.50$ = 164 kNm.

8. For this configuration, the friction coefficient, μ, is 0.30 for steel shims of the type tested, the bolt diameter, d, is 16 mm, the lever arm, l, is 10 mm + 2 x 3 mm/shim + $0.2d$ = 19.2 mm, and f_{uf} = 830 MPa so the coefficients in Equation 10 are a = -0.8640, b = 443,935, and c = -25,282,740,224 and N = 64.6 kN, so V = 64.6 x 0.30 = 19.4 kN/bolt/surface = 38.8 kN/bolt, and the normalized shear resistance/bolt/surface is μ_n = 19.4 kN/95 kN = 0.20, where 95 kN is the bolt proof load. This result can be checked with Equation 5 and it may be found that $M^*/M_{rfn} + V^*/V_{fn} = 0.737 + 0.263 = 1.0$.

9. If the bolts providing moment resistance in the web are at 251 mm from the top of the beam, and 4 bolts are provided in a line in the web and in each side of the bottom flange, then the total moment resistance M_{slide} is 38.8 kN x 4 x 360 mm x 2 + 38.8 kN x 4bolts x 251 mm = 150 kNm. This is less than $M_{slide,max}$ so it is satisfactory.

10. M_{des} is 135 kNm

11. The horizontal force on top flange plate and bolts is (38.8 kNx4x2 + 38.8 kNx4) = 466 kN. For the M16 8.8N bolts, with threads included in the shear plane, ϕV_{fn} = 59.3 kN per bolt, meaning that 7.9 bolts are required. For practical considerations, two rows of 4 bolts per row are required

12. The beam shear demand V_{beam} is 150 kNmx1.4/1.5 m = 140 kN. Four M16N Property Class 8.8 bolts in one row at the top web plate in ordinary (non-elongated) holes will be sufficient as their individual single shear capacity,

threads included, is 59.3 kN. In practice there will be additional shear from the gravity loading which may require further bolts.

8. CONCLUSIONS

This paper describes systems to minimize structural damage during strong earthquake shaking and introduces the concept of the sliding hinge joint. It is shown that:

1) The sliding hinge joint is an inexpensive and innovative way to minimize structural damage to the whole structural system, including the lateral resisting frames and the floor slab during earthquake shaking. For these reasons it may be referred to as a Generation 4 connection. The joint dissipates energy on double friction surfaces and the resulting hysteresis loop demonstrates a low possibility of large permanent displacements. It has the further advantage that it costs a similar amount to fabricate and erect as conventional connection and high quality control may be maintained with shop welding and site bolting. For these reasons it is already used in construction of buildings in New Zealand.

2) Materials other than brass are effective as shim materials at the sliding interfaces. Aluminium has greater frictional resistance, but this drops with repeated cycles of loading. Steel shims have similar behaviour to brass shims, but are cheaper, more readily available, less likely to cause corrosion problems due to dissimilar metal problems, and can be tack welded into position for easy erection.

3) The compressive force over the sliding interface is related to axial force in the bolts. This in turn is affected by the initial fully tensioned bolt load, and the moment-shear-axial force interactions which occur as the bolts drag the floating cap plates. Simple expressions for estimating the final normal compression were developed.

4) Construction tolerances affect the initial force that can be applied to the interface. For the case studied, the construction tolerances affected the interface compressive force by only about 6%.

5) A simple methodology for design of these frames is presented and a design example is provided.

9. FUTURE RESEARCH

The following aspects of sliding joint performance should be investigated:

1) The effect of long term durability of the sliding surfaces needs to be investigated before the joint can be used in other than dry, internal environments.

2) Once the SHJ has undergone sliding the joint is permanently softened. The extent and effect of this needs to be better quantified.

3) All research to date has been on galvanized property class 8.8 high strength structural bolts which are fully tensioned into the inelastic range by the turn of the nut method. The SHJ performance with other types of bolts should be investigated. For example, black bolts of a higher property class, such as grade 12.9, tensioned to 60% of the proof load may remain elastic during the sliding and they would be easier to install. They may also provide better control of the tension force in the bolt than is possible with galvanized bolts.

4) The SHJ concept should be applied to other types of connection, such as those in braced members, in shear links, or as couplers between walls or frames. Studies are required to validate possible approaches and develop design solutions.

This research is currently underway at the Universities of Auckland and Canterbury.

ACKNOWLEDGEMENTS

The authors are grateful for the test units provided by John Jones Steel Limited, and for the advice and encouragement from the New Zealand Heavy Engineering Research Association, HERA. Partial funding for this work was provided by the University of Canterbury and the FRST-funded Program Retrofit solution for NZ Multi-storey Buildings. This support is gratefully acknowledged. All opinions expressed in this paper are those of the authors and do not necessarily represent those of the sponsors.

REFERENCES

1 Mackinven, H., MacRae, G.A., Pampanin, S., Clifton, G.C., Butterworth, J. Generation Four Steel Moment Frame Joints, *Proceedings of the Pacific Conference on Earthquake Engineering* (PCEE), Paper 200, Singapore, 05 – 07, December 2007.

2 Housner, G. The Behavior of Inverted Pendulum Structures during Earthquakes. *Bulletin of the Seismological Society of America* 1963; **53**(2); 403-417.

3 Robinson, W.H. and Greenbank, L.R. An extrusion energy absorber suitable for the protection of structures during an earthquake. *Earthquake Eng. Structural. Dynamics* 1976; **4;** 251–259.

4 Pall, A.S., Marsh, C., Fazio, P. Friction Joints for Seismic Control of Large Panel Structures, *Journal of the Precast concrete Institute*, 1980; **25** (6); 38-61.

5 Christopoulos, C., Filiautrault, A. Principles of Passive Supplemental Damping and Passive Isolation, *IUSS PRESS, Pavia* – Italy, 2006.

6 Arima, F., Miyazaki, M., Tanaka, H., Yamazaki, Y. A Study on Buildings with Large Damping Using Viscous Damping Walls, *Proc. 9th World Conference on Earthquake Engineering*, Tokyo/Kyoto, Japan, 1988.

7 Cheok, G., Stone, W., Lew, H.S. Partially Prestressed and Debonded Precast Concrete Beam-Column Joints, *Proceedings of the 3rd Meeting of the US-Japan Joint Technology Coordinating Committee on Precast Seismic Structural Systems*, November 1992.

8 Priestley, M.J.N. and MacRae, G.A. Seismic Tests of Precast Beam-to-Column Joint Subassemblages with Unbonded Tendons, *PCI Journal*, January-February 1996; 64-80.

9 Priestley, M.J.N. The PRESSS program - current status and proposed plans for Phase III, *PCI Journal*. Mar.-Apr 1996, 41(2); 22-40.

10 Priestley, M.J.N., Sritharan, S., Conley, J.R., Pampanin, S. Preliminary Results and Conclusions from the PRESSS Five-Storey Precast Concrete Test Building, *PCI Journal*, Nov-Dec 1999; **44**(6); 42-67.

11 Umarani, C., MacRae, G.A. A New Concept For Consideration Of Slab Effects On Building Seismic Performance, Journal of Structural Engineering,

Structural Engineering Research Centre, Chennai, India, No. 34-3, April-May 2007; **34**(1); 25–32.

12 Danner, M., Clifton, G.C. Development of Moment-Resisting Steel Frames Incorporating Semi-Rigid Elastic Joints: Research Report; *HERA*, Manukau City, New Zealand, Report R4-87, 1995.

13 Christopoulos, C., Filiatrault, A., Uang, C.M., Folz, B. Post-tensioned Energy issipating Connections for Moment Resisting Steel Frames, *ASCE Journal of Structural Engineering*, 2002; **128**(9); 1111-1120.

14 Ricles, J., Sause, R., Peng, S., Lu, L. Experimental Evaluation of Earthquake Resistant Posttensioned Steel Connections, *Journal of Structural Engineering, American Society of Civil Engineering*, 2002; **128**(7); 850-859.

15 Clifton, G.C. Semi-Rigid joints for moment resisting steel framed seismic resisting systems. PhD Thesis, *Department of Civil and Environmental Engineering, University of Auckland,* 2005.

16 Fenwick, R.C., Megget, L.M. Elongation and Load Deflection Characteristics of Reinforced Concrete Members containing Plastic Hinges. *Bulletin of the New Zealand National Society for Earthquake Engineering*, 1993; **26**(1); 28-41.

17 Clifton, G.C. Development of Perimeter Moment-Resisting Steel Frames Incorporating Semi-Rigid Elastic Joints, *New Zealand National Society for Earthquake Engineering Conference*, 1996;177-184.

18 Mander, T.J. Seismic Resistance of Rigid Structural Steel Beam-Column Connections Designed for Damage Avoidance, Undergraduate Project Report, Civil Engineering, *University of Canterbury*, Christchurch, 2007.

19 Kishiki, S., Suzuki, K., Yamada, S., Wada, A. Shear Transfer Mechanism Based on Connection Elements at the Top Flange of Beams Ends, *Pacific Structural Steel Conference*, Wairakei, New Zealand, 13-16 March 2007.

20 Pampanin, S., Amaris, A., Akguzel, U., Palermo, A. Experimental Investigations on High-Performance Jointed Ductile Connections for Precast Frames. Proceedings of the *First European Conference on Earthquake Engineering and Seismology*. Geneva, Switzerland, 2006.

21 Amaris, A., Pampanin, S., Bull, D., Carr, A.J. Development of a Non-tearing Floor Solution for Jointed Precast Frame Systems, *Proc. National Society for Earthquake Engineering,* Palmerston North, New Zealand, 2007.

22 Gledhill, S.M., Sidwell, G.K., Bell, D.K. The Damage Avoidance Design of Tall Steel Frame Buildings - Fairlie Terrace Student Accommodation Project, Victoria University of Wellington, *New Zealand Society of Earthquake Engineering Annual Conference*, Wairakei, April 2008.

23 Takanashi, K., Tanaka. H., Taniguchi, H. Influence of Slipping at High Strength on Dynamic Behaviour of Frames. Joints in Structural Steelwork: Proceedings of the International Conference on Connections. *Pentech Press, UK*, 1981.

24 Grigorian, C.E., Popov, E.P. Energy Dissipation with Slotted Bolted Connections. *Engineering Research Center* Report No. UCB/EERC-94/02, Berkeley, CA, USA, 1994.

25 De la Cruz, S.T., Lopez-Almansa, F., Taylor, C. Tests of Friction Energy Dissipators for Seismic Protection of Building Structures, *8th World Seminar on Seismic Isolation, Energy Dissipation and Active Vibration Control of Structures*, Yerevan, Armenia, October 2003.

26 AS/NZS 1252. High Strength Steel Bolts with Associated Nuts and Washers for Structural Engineering, Standards New Zealand, Wellington, New Zealand, 2006.

27 Clifton, G.C., MacRae, G.A., Mackinven, H., Pampanin, S., Butterworth, J. Sliding Hinge Joints and Subassemblies for Steel Moment Frames, *New Zealand Society for Earthquake Engineering Annual Conference*, Paper 19, Palmerston North, 2007.

28 MacRae, G.A., P-Delta Effects on Single-Degree-of-Freedom Structures in Earthquakes, *Earthquake Spectra*, August 1994; **10**(3); 539-568.

29 Kawashima, K., MacRae, G.A., Hoshikuma, J., Nagaya, K. Residual Displacement Response Spectrum, *ASCE Journal of Structural Engineering*, ASCE, May 1998, pp. 523-530.

30 NZS 3404. Steel Structures Standard, Incorporating Amendments 1 and 2, Standards New Zealand, Wellington, New Zealand, 2007.

31 Mackinven, H. Sliding Hinge Joint for Steel Moment Frames Experimental Testing, ENCI 493 Project Report, *Department of Civil Engineering, University of Canterbury*, 2006.

32 MacRae, G.A., MacKinven, H., Clifton, G.C., Pampanin, S., Walpole, W.R., Butterworth, J. Tests Of Sliding Hinge Joints For Steel Moment Frames, *Pacific Structural Steel Conference*, Wairakei, NZ, 2007.